



Is the local seismicity in western Hispaniola (Haiti) capable of imaging northern Caribbean subduction?

J. Corbeau^{1,2,*}, O.L. Gonzalez^{3,*}, V. Clouard^{1,2,*}, F. Rolandone^{4,*}, S. Leroy^{4,*}, D. Keir^{5,6,*}, G. Stuart^{7,*}, R. Momplaisir^{8,*}, D. Boisson^{8,*}, and C. Prépetit^{9,*}

¹Université de Paris, Institut de Physique du Globe de Paris, Centre national de la recherche scientifique (CNRS), UMR 7154, F-97250 Saint-Pierre, France

²Observatoire Volcanologique et Sismologique de Martinique, Institut de Physique du Globe de Paris, Centre national de la recherche scientifique (CNRS), F-97250 Saint-Pierre, France

³Centro Nacional de Investigaciones Sismológicas (CENAI), Ministerio de Ciencia, Tecnología y Medio Ambiente, Santiago de Cuba 90400, Cuba

⁴Sorbonne Université, Centre national de la recherche scientifique–Institut national des Sciences de l'Univers (CNRS-INSU), Institut des Sciences de la Terre Paris (ISTeP), Paris, France

⁵School of Ocean and Earth Science, University of Southampton, European Way, Southampton SO14 3ZH, UK

⁶Dipartimento di Scienze della Terra, Università degli Studi di Firenze, Florence 50121, Italy

⁷Institute of Geophysics and Tectonics, School of Earth and Environment, University of Leeds LS2 9JT, UK

⁸Université d'Etat d'Haiti, Faculté des Sciences, HT 6112 Port-au-Prince, Haiti

⁹Unité Technique de Sismologie, Bureau des Mines et de L'Energie, HT 6120 Port-au-Prince, Haiti

ABSTRACT

The boundary between the Caribbean and North American plates in the Hispaniola region is the northwestern termination of the North American plate subduction evolving from westward subduction in the Lesser Antilles to southward subduction in the Greater Antilles and oblique collision against the Bahamas platform in Cuba. We analyze P waveforms recorded by 27 broadband seismic temporary stations deployed during the Trans-Haiti project. Seismicity recorded by the temporary network from June 2013 to June 2014 is used to locate the earthquakes. A total of 514 events were identified with magnitudes ranging from 1 to 4.5. Twenty-six moment tensors were calculated by full waveform inversion using the ISOLA software. The analysis of the new moment tensors for the Haiti upper lithosphere indicates that normal, thrust and strike-slip faulting are present but with a majority of thrust faulting. The mean P and T axes for the moment tensors indicated that the current compressional deformation is mainly N-S to NNE-SSW. Moreover, a dozen intermediate-depth earthquakes (>70 km) are located under Haiti, with one event in the south of the island reaching 260 km depth. The seismic data of the Haiti network, over a one-year time period, tend to confirm the existence of a lithospheric slab inherited from southward subduction under the Greater Antilles. The scarcity of the intermediate-depth seismic events in this area may be the effect of the lack of a dense seismic network or may indicate that we image the western slab edge.

1. INTRODUCTION

Recently, the Mw 7.0 2010 Haiti transpressional earthquake prompted several geological and geophysical studies to constrain the fault geometry and

*E-mail: corbeau@ipgp.fr; oleary@cenais.cu; clouard@ipgp.fr; frederique.rolandone@sorbonne-universite.fr; sylvie.leroy@sorbonne-universite.fr; D.Keir@soton.ac.uk; G.W.Stuart@leeds.ac.uk; roberte.momplaisir@laposte.net; dmbouisson@yahoo.com; claudprepetit@hotmail.com

the crustal structure in the area of the main shock near the capital city Port-au-Prince (Calais et al., 2010; Mercier de Lépinay et al., 2011; Douilly et al., 2013; Leroy et al., 2015). However, as sadly reminded by the 7 October 2018 Mw 5.9 and Mw 5.4 earthquakes occurring in the north of Haiti, our knowledge of the local seismicity remains very limited in the absence of a dense permanent seismic network in Haiti. Many questions remain unresolved, as for example where the current deformation is accommodated at the surface and at depth, and if there is a subducting slab or a remnant slab under Haiti.

The Trans-Haiti project, a temporary seismic network consisting of 27 stations, was deployed in Haiti from April 2013 for nearly 14 months to record the local seismicity. Local events over a period of one year have been located, and associated focal mechanisms have been computed. In addition, we analyzed seismograms from five permanent stations in Haiti and from 15 other stations in Cuba, Jamaica, Dominican Republic, and Bahamas to improve the network coverage in this period of time. The precise knowledge of seismic source parameters (such as earthquake location and fault-plane solution) is a key for understanding physical processes on faults during earthquakes and regional deformation style.

This paper focuses on the local seismicity using the Trans-Haiti temporary network of 27 seismometers crosscutting Haiti. The aim of this study is to determine where the most active faults are located and the current type of faulting based on focal mechanisms. We use the local seismicity to improve the knowledge of the crustal structure of Haiti and to constrain what happens deeper in the lithosphere.

2. STRUCTURAL SETTING AND PREVIOUS STUDIES

Haiti, the western part of Hispaniola Island, is located at the boundary between the North American plate and the Caribbean plate (Fig. 1). Haiti is a part of the Cretaceous volcanic island arc formed at the boundary of the Pacific realm called the Greater Antilles arc (Burke, 1988; Pindell et al., 2006).

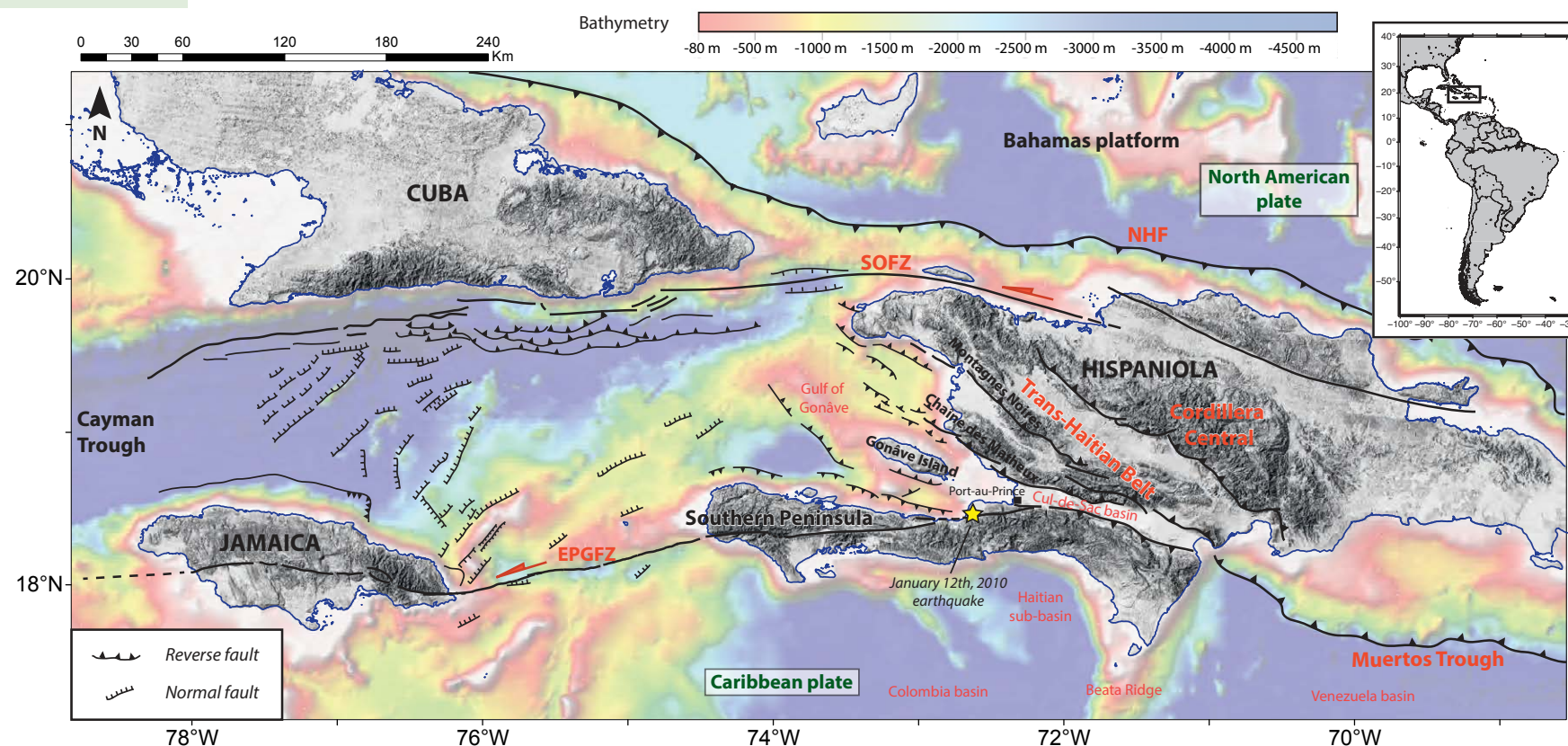


Figure 1. Tectonic map of the northern Caribbean plate boundary in the Hispaniola region. NHF—North Haitian fault; SOFZ—Septentrional-Oriente fault zone; EPGFZ—Enriquillo-Plantain-Garden fault zone. Faults are from previous studies (Calais and Mercier de Lépinay, 1991; Mann et al., 1995; Leroy et al., 1996, 2015; Granja-Bruña et al., 2014).

The Greater Antilles arc now consists of part of Cuba, Hispaniola, and Puerto Rico islands (Mann et al., 1995). It constitutes two-thirds of Hispaniola Island and is mainly made up of arc magmatic facies (Boisson, 1987; Escuder-Viruete et al., 2006). The Greater Antilles arc became an inactive intra-oceanic arc at the end of the Late Cretaceous when it collided with the Bahamas carbonate platform (Leroy et al., 2000; Iturralde-Vinent, 2006; Cruz-Orosa et al., 2012).

Currently, the boundary between Hispaniola and the North American plate is the northwestern termination of the Lesser Antilles subduction zone, as the west-dipping subduction under the Lesser Antilles transitions into a south-dipping subduction beneath Hispaniola and Puerto Rico (McCann and Sykes, 1984). However, this south-dipping subduction is interpreted to end in the middle of Hispaniola, a hypothesis based on the absence of deep seismicity (Symithe et

al., 2015). Therefore, the plate boundary in western Hispaniola is interpreted to instead be an oblique collision.

The oblique motion of the Caribbean plate occurs at ~20 mm/yr toward the NE relative to the North American plate (Calais et al., 2002). The transpressional deformation is partitioned between several strike-slip and thrusting structures. In Haiti, the main structures are (from N to S) the North Haitian thrust fault, the sinistral strike-slip Septentrional-Oriente fault zone, the Trans-Haitian fold and thrust belt, and the sinistral strike-slip Enriquillo-Plantain-Garden fault zone (Fig. 1). A block modeling study based on GPS data shows that the movement is currently transpressional on the Enriquillo-Plantain-Garden fault zone, with a major compressional component, while it is mainly strike-slip on the Septentrional-Oriente fault zone (Benford et al., 2012). Another study with

an improved data set (Symithe and Calais, 2016) shows that the active strain accumulation in the southern part of the island involves an additional significant component of N-S shortening. A seismic-reflection study indicates that several active thrusts are present offshore in the Gulf of Gonâve (Corbeau et al., 2016). A receiver function study finds that the depth of the Moho across Haiti is variable, ranging from 16 to 45 km, and that three distinct crustal terranes are accreted along the plate boundary (Corbeau et al., 2017).

3. DATA AND METHOD

3.1 Data

Data come from the Trans-Haiti temporary network that was deployed in Haiti in April 2013 and recorded until June 2014 (Fig. 2). We installed 27 broadband stations (11 CMG-6TD and 16 CMG-40 TD), mainly along a north-south profile to image the crustal structure of western Hispaniola (Corbeau et al., 2017). A number of stations are also geographically distributed and complement the five permanent broadband stations from the Bureau des Mines et de l'Énergie (BME) and the Natural Resources of Canada (NRCAN) to characterize the local seismicity. When data are available, we also add the records of stations from Dominican Republic, Cuba, Bahamas, and Jamaica (Fig. 2) to improve the event locations and the focal mechanism inversions.

3.2 Location of Seismic Events

We use the SeisComp3 software for our events database (Hanka et al., 2010). To automatically detect the seismic events on the stations records, we use a new application, Seismic Data Playback code (SDP), developed at the Observatoire Volcanologique et Sismologique de Martinique, Institut de Physique du Globe de Paris (OVSM-IPGP) (SDP is available on GitHub, <https://github.com/ovsm-dev/sdp>). The SDP interface is still under development, and this is the first time that it has been used on real data (Supplemental File¹). It comprises a semi-automatic interface for the postcampaign seismic data processing. It enables fast reading of the data and the automatic extraction of potential seismic events that are detected with a short-time average/long-time average (STA/LTA) filter. It generates Python ObsPy code for the offline analysis of seismic data (Beyreuther et al., 2010). When two distinct pulses are identified (P and S waves) on at least three stations, a seismic event is considered on the related portion of the seismogram. Trans-Haiti data are relatively noisy, and the specific north-south distribution of the seismic stations result in a high dependency of the triggering events on the choice of the STA/LTA parameters. Typically, we ran SDP with the set of STA/LTA parameters of 2.8 s and 22.5 s, respectively (footnote 1). Triggered events are then visually validated and sent to the SeisComp3 interface scolv. The P and S phases are then manually picked and earthquake locations are computed with HYPO71 (Lee and Lahr, 1972), NonLinLoc (Lomax et al., 2000), and LOCSAT. The locations

Supplemental File
Seismic Data Playback (SDP)

1. Overview

Seismic Data Playback (SDP) is a code developed at the OVSM-IPGP (Observatoire Volcanologique et Sismologique de Martinique - Institut de Physique du Globe de Paris). It is available on the GitHub platform, at the address <https://github.com/ovsm-dev/sdp>.

SDP is a semi-automatic interface for the post-campaign seismic data processing. It detects and extracts seismic events on past seismic records, and sends them on a SeisComp3 database to allow their localizations. It uses Python 2.7 and the ObsPy toolbox. SDP is based on the 'short-time-average through long-time-average trigger' (STA/LTA) that is the most broadly used algorithm in weak-motion seismology (Trehub, 2012). It continuously calculates the average values of the absolute amplitude of a seismic signal in two consecutive moving time windows. The short time window (STA) is sensitive to seismic events while the long time window (LTA) provides information about the temporal amplitude of seismic noise at the site. When the ratio of both exceeds a pre-set value, an event is 'declared' and data starts being recorded in a file.

2. Parameters

SDP code is based on a STA/LTA ratio which depends on 5 parameters:

- STA (Short Time Average)
- LTA (Long Time Average)
- Threshold ON (Trigger)
- Threshold OFF (Detrigger)
- Threshold SUM

STA and LTA are average absolute amplitudes over short and long periods of time respectively. User chooses the short and long periods of time in seconds, with STA always lower than LTA. Threshold ON parameter corresponds to the minimum value of ratio STA/LTA for which the beginning of a seismic event is considered. Threshold OFF parameter is the ratio value that determines the end of the seismic event. Threshold SUM parameter is the minimum number of stations that should have recorded the seismic event to save it.

3. Optimization of the parameters

Several tests were done to choose appropriate parameters for Trans-Haiti data. Trans-Haiti data are relatively noisy and the specific north-south distribution of the seismic stations result in a high dependency of the triggering events on the choice of the STA/LTA parameters. For example, we used visualization software to select a 12 hours period with a high number of seismic events. We selected the January 20th 2014 from 06:00 am to 06:00 pm where 6 seismic events were identified.

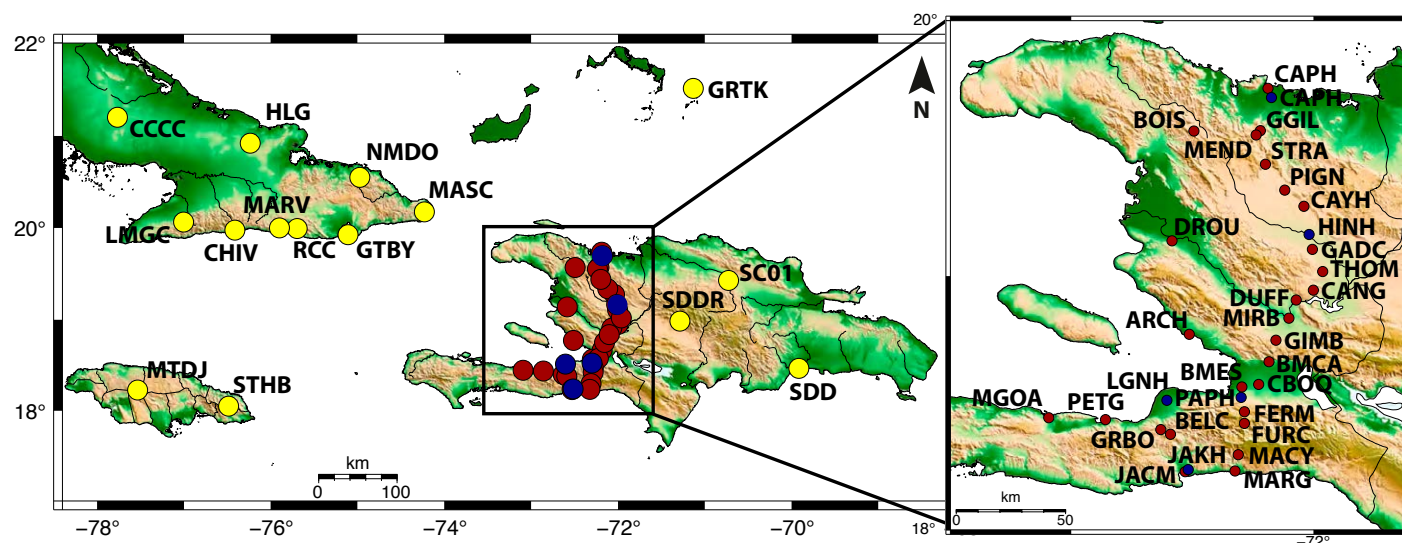


Figure 2. Map of the stations used in this study. The red dots are the temporary seismic stations of the Trans-Haiti network deployed from 2013 to 2014. The blue dots are the Haitian permanent stations of the Canadian network. The yellow dots are permanent stations from Cuba, Jamaica, Bahamas, and Dominican Republic.

¹Supplemental File. Overview, parameters, and optimization of the parameters for Seismic Data Playback (SDP) software. Please visit <https://doi.org/10.1130/GES02083.S1> or access the full-text article on www.gsapubs.org to view the Supplemental File.

are accepted when the root mean square (RMS) travel time residual is <0.35 . Crustal velocity models exist for Haiti but only for the southern part of the island (Douilly et al., 2013). However, Corbeau et al. (2017) show that the Moho depth and the crustal composition are highly variable across Haiti. A velocity model applicable only for the southern part could not be used for the whole island, and we use a crustal velocity model adapted from the Dorel (1978) model that is used in the Lesser Antilles. This 1D model consists of three crustal layers with 3, 15, and 30 km of thicknesses and V_p (P velocities) of 3.5, 6.0, and 7.0 km/s. The mantle is then represented by a half space with a P velocity of 8.0 km/s, and the V_p/V_s ratio is 1.76 for all the layers. Finally, we compute the duration magnitude for $M < 3.5$ and the local magnitude on the vertical components, M_{lv} for $M > 3.5$.

3.3 Focal Mechanisms Calculations

To compute focal mechanisms by full waveform inversion, we use the software package ISOLA-GUI (Sokos and Zahradnik, 2008). The methodology is based on the iterative deconvolution technique, adjusted for regional and local distances. Prior to the inversion process, we inspect all the data to choose only the events where P and S waves are well identified. We use ISOLA to pre-process the data (integration, instrument correction, origin alignment, and signal to noise ratio). Stations with inconsistent results are removed from the data set. For the waveform inversion, we use the same velocity model as for the location of the seismic events (see section 3.2). Density values are from Nafe and Drake (1960), and attenuation quality factors Q_p and Q_s are from Graves and Pitarka (2010), with $Q_s = 50 V_s$ and $Q_p = 2 Q_s$.

The moment tensors are calculated during the full waveform inversion by a least squares method. In addition, centroid position and time are also calculated by grid searching. We first performed a spatial grid search vertically on trial sources around the hypocenter (step of 1 km) and in an interval of ± 3 s around the origin time (step of 0.09 s). This gives us an approximation of the source depth (Fig. 3A). Then a second grid search is performed on a plane around the depth preferred in the first grid search, with steps of 1 km. The inversion frequencies are chosen as a function of the hypocentral distances and the magnitudes of the events (Sokos and Zahradnik, 2013).

Several parameters are plotted after the inversion to estimate the robustness of the solution. We first plot the synthetic waveforms, generated for the calculated moment tensor solution, versus the observed waveform from the real seismogram (Fig. 3B). The Kagan angle describes in one single value the deviation of a given solution from the reference solution (deviations of strike, dip, and rake). The Kagan angle value of lower than 15 represents good stability of the solution (Zahradnik and Custódio, 2012). In addition, the condition number (CN) is useful in judging how well the inverse problem is posed, large CN > 10 indicating an unstable solution (Křížová et al., 2013). We selected only the inversions for which at least nine components are used and with a signal to noise ratio of a minimum of 2. Finally, variance reduction (VR)

and double-couple percentage (DC) also characterize the best-fitting solution. These values should both be as high as possible and always $> 30\%$.

3.4 Calibration

In order to check the validity of the velocity model and the inversion parameters, we relocate a TNT shot and a Mw 5.8 earthquake identified by the global catalogs (U.S. Geological Survey [USGS] and Centroid Moment Tensor [GCMT]). The Mw 5.8 earthquake occurred 28 May 2014 in the Mona Passage between Hispaniola and Puerto Rico. The different locations and the associated focal mechanisms from GCMT, USGS, and our study are indicated in Table 1. The GCMT and USGS epicenters are separated by 39 km, and the hypocenters are at depths of 89 km and 100.5 km, respectively. By comparison, the epicenter calculated in our study is 46 km from the GCMT solution, and our hypocenter is 16 km deeper (105 km versus 89 km for the GCMT solution). Our epicenter is also 44 km away from the USGS epicenter, and our hypocenter is 4.5 km deeper. Although the locations differ, they are in the same range of variability. The magnitudes are the same (Mw 5.8), and the three moment tensors are similar (maximum 13° , 8° , and 12° of variability in the strike, dip, and rake, respectively), validating our choice of inversion parameters used for the focal mechanism. The TNT shot was made 28 November 2013 in Dominican Republic, the eastern part of Hispaniola Island, near the Haitian border. From our seismic data, we locate this event at 3 km from its actual location, and only 400 m deeper (Table 1). The RMS of our location is 0.03 with horizontal and vertical error bars of 1 km and 3 km, respectively, which indicates that the velocity model we use is sensible. We conclude that our locations and inversion parameters retrieve robust moment tensors.

4. RESULTS

4.1 Local Seismicity

From June 2013 to June 2014, we have located 514 seismic events in Haiti with magnitudes ranging from 1 to 4.5 (Fig. 4). These earthquakes are predominantly shallow (< 20 km), and several clusters can be identified in the south of the study area. Two clusters are located at the eastern and western extremities of a fault model proposed by Mercier de Lépinay et al. (2011) for the 2010 Mw 7.0 earthquake, aligned along the Enriquillo-Plantain-Garden fault zone surface trace. A cluster of small magnitude events exists in the extreme south of Haiti, near the border with the Dominican Republic, in an area shifted to the south of Enriquillo-Plantain-Garden fault zone. Just behind the Haitian border, in Dominican Republic, a cluster of seismic events is identified along the northern side of the Enriquillo Lake (enlargement in Fig. 4): in June and July 2013, 51 earthquakes occurred with magnitudes ranging from 2.3 to 3.8 and depths ranging from 1 km to 33 km. To the north, small seismic clusters

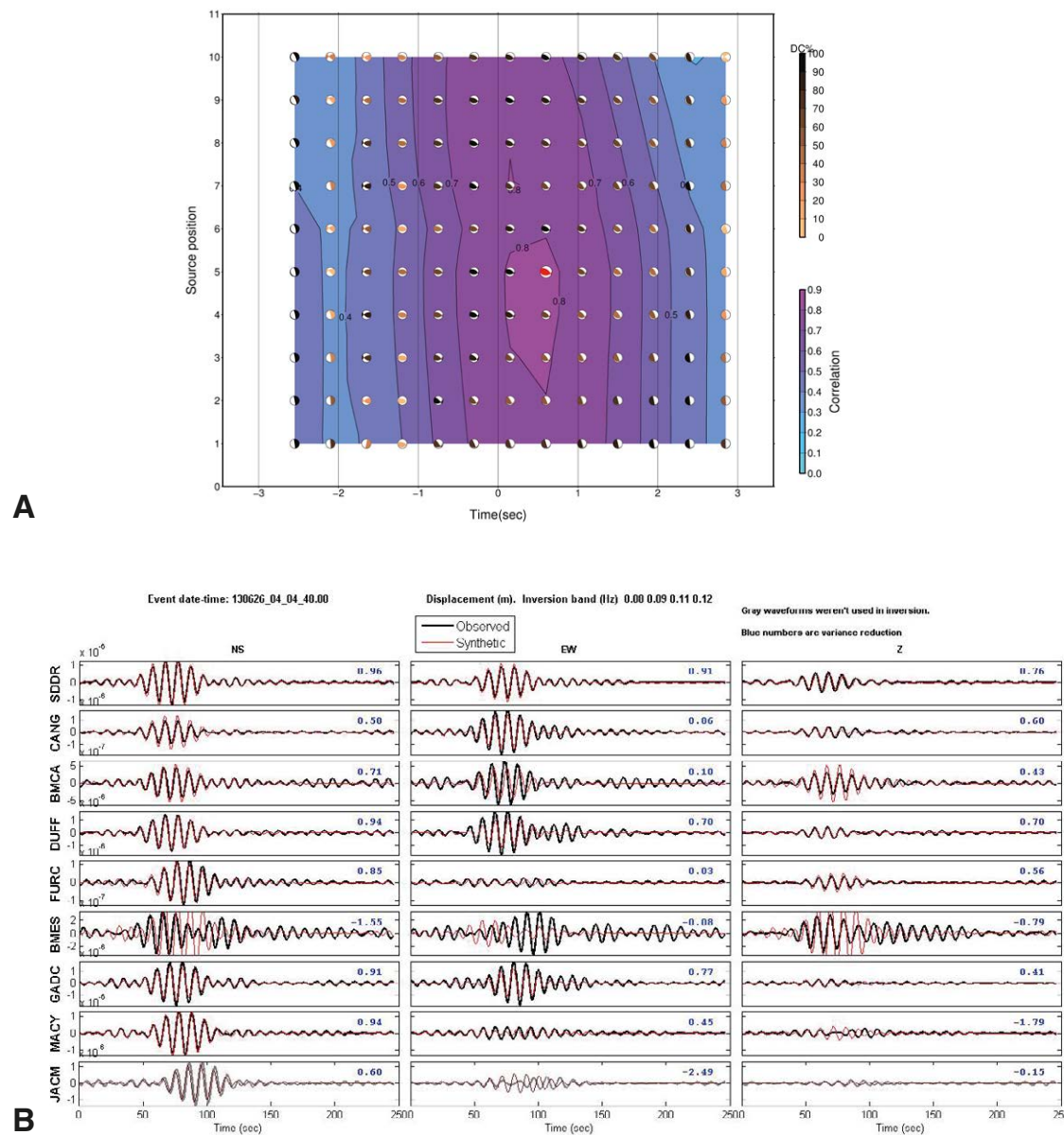


Figure 3. (A) Representation of a vertical grid search for the 26 June 2013 04:04:48 UTC earthquake. The vertical grid search is done in ten trial positions around the hypocenter (starting depth is 1 km and vertical step is 1 km) and around the origin time (the range is ± 3 s with a step of 0.45 s). The best-fitting solution is represented by the red beach ball (largest correlation). The color of the other beach balls represents the double-couple percentage (DC%). This is a representative example for the clarity of the grid. The steps used in this study are mentioned in the text section 3.3. (B) Example of the synthetic waveforms (in red) versus the observed waveform (in black) for the 26 June 2013 04:04:48 UTC earthquake. The variance reduction values are indicated in blue for each component.

TABLE 1. COMPARISON OF HYPOCENTERS AND FAULT-PLANE SOLUTIONS FOR 28 MAY 2014 M5.8 EVENT BETWEEN OUR STUDY AND GCMT AND USGS CATALOGS; COMPARISON BETWEEN POSITION OF TNT SHOT AND ITS LOCALIZATION WITH OUR DATA SET

Event no.	Origin time yyymmdd hh:mm:ss.ss	Lat	Long	Depth	Mw	NP1			NP2			Mom Ten	DC%	VR%	NC	SNR	K°	CN
						Strike	Dip	Rake	Strike	Dip	Rake							
This study	20140528 21:15:01.00	18.22	-67.97	105.0	5.8	34	23	56	250	71	103		98.6	52	18	44	5.4	4.5
CGMT	20140528 21:15:07.90	18.40	-68.36	89.0	5.8	29	30	44	259	69	113							
USGS	20140528 21:15:06.00	18.05	-68.35	100.5	5.8	36	31	48	263	68	112							
This study	20131128 19:28:48.00	18.98	-71.81	0.5	3													
TNT shot	20131128	18.98	-71.78	0.1														

Notes: DC%—double-couple percentage; VR%—variance reduction percentage; NC—number of components used; SNR—signal to noise ratio; K°—mean Kagan angle; CN—condition number; GCMT—Global Centroid Moment Tensor; Mom Ten—Moment tensor; USGS—U.S. Geological Survey.

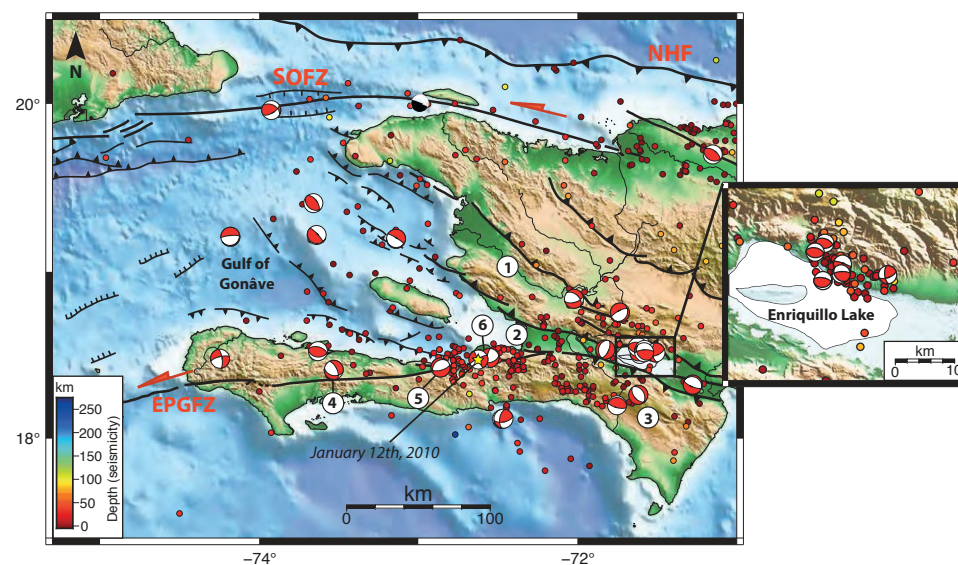


Figure 4. Local seismicity in Haiti from June 2013 to June 2014 and focal mechanisms calculated in this study. The black focal mechanism in the north of Haiti is from GEOSCOPE Observatory and related to the 7 October 2018 event. NHF—North Haitian fault; SOFZ—Septentrional-Oriente fault zone; EPGFZ—Enriquillo-Plantain-Garden fault zone. Enlargement: Enriquillo Lake. Numbers are for: 1—Artibonite Valley; 2—Cul-de-Sac Basin; 3—Sierra de Bahoruco; 4—L'Asile Basin; 5—Miragoâne Lake; and 6—Leogâne fan delta.

are present at the eastern end of the Septentrional-Oriente fault zone. Apart from these clusters, diffuse seismicity is observed, offshore in the Gulf of Gonâve and along the Septentrional-Oriente and the North Haitian faults in the north of the island.

4.2 Focal Mechanisms

Using the ISOLA software, 19 focal mechanisms were calculated with the Trans-Haiti network data (Fig. 4; Table 2). We added seven focal mechanisms calculated by the regional network data from 2015 to 2017 to improve the coverage offshore (Fig. 4; Table 3). Of the 26 focal mechanisms calculated in this study, 14 are shallow (depths <10 km) with epicenters on land; eight are located at depths between 10 and 20 km and located along the Enriquillo-Plantain-Garden fault zone; and four are located offshore at depths from 20 to 30 km (Fig. 5A). Fourteen focal mechanisms are compressional, ten are extensional, and two are strike-slip (Fig. 5B). The P and T axes of the 26 centroids are plotted on rose diagrams (Fig. 6). The average P azimuth is ~15° (NNE-SSW), while the T axes do not have a very consistent direction, although NE-SW is the most dominant.

5. INTERPRETATIONS AND DISCUSSION

5.1 Current Deformation

Only two left-lateral strike-slip focal mechanisms are identified on the 26 focal mechanisms calculated in this study. They are located along the Enriquillo-Plantain-Garden fault zone (events 24 and 9; Fig. 5A) and associated with an adjacent fault (event 24; Mann et al., 1995) and the fault zone itself near the location of the 2010 earthquake (event 9). The scarcity of this type of event is surprising in this area where a majority of the current deformation is supposed to be strike-slip (Calais et al., 2010; Benford et al., 2012).

Of the 26 focal mechanisms calculated in this study, ten are normal or transtensional (Fig. 5B). On the Southern Peninsula of Haiti, three normal focal mechanisms are aligned along the Enriquillo-Plantain-Garden fault zone (events 10, 18, and 19; Fig. 5A). From west to east, they correspond to extensional deformation in L'Asile Basin, the Miragoâne Lake, and the Leogâne Quaternary fan delta (Fig. 4) (Mann et al., 1995; Wang et al., 2018); these examples of extensional deformation correspond to extensional stepovers or pull-apart basins along the sinistral strike-slip Enriquillo-Plantain-Garden fault zone. Farther east in the Cul-de-Sac basin (Fig. 4), two normal focal mechanisms are also identified on both sides of the Enriquillo Lake (events 15 and 13; Fig. 5A) and may be related to normal faults that were mapped previously by Pubellier et al. (2000) in this area. South of the Enriquillo Lake, a normal focal mechanism (event 2; Fig. 5A) can be associated with the collapse of the Sierra de Bahoruco (Fig. 4) along large normal faults (Pubellier et al., 2000).




















North of the Cul-de-Sac basin, the two other normal focal mechanisms (events 26 and 16; Fig. 5A) can be interpreted as extensional fractures on the upper side of folds (extrados faults) or the termination of the subsiding Artibonite valley (Pubellier et al., 2000) (Fig. 4). Offshore in Gulf of Gonâve, two other normal focal mechanisms are identified (events 25 and 22; Fig. 5A). Event 25, at 30 km depth, can be associated with the extensional deformation in half-graben mapped in this area (Leroy et al., 2000). Finally, event 22 at 9 km depth can be associated with the flat fault ramps identified previously in the Gulf of Gonâve (Corbeau et al., 2016).

A majority of the 26 focal mechanisms are thrust-fault related (Fig. 5B). In the Gulf of Gonâve, two thrusts are identified (events 20 and 21; Fig. 5A) and are well correlated with the active compressional deformation mapped in this area by seismic profiles (Corbeau et al., 2016). There are three thrusting events identified on the borders of the Southern Peninsula, one in the north and two in the south (events 17, 12 and 11; Figs. 5A and 5B). In the north, thrusts faults were previously imaged with seismic-reflection studies (Bien-Aimé Momplaisir, 1986; Corbeau et al., 2016) and correspond to the thrusting of the Southern Peninsula in the Gulf of Gonâve. In the south, transpressional faults oriented N90° were also imaged by Bien-Aimé Momplaisir (1986) and Mauffret and Leroy (1999) and can be related with events 12 and 11 of this study. Finally, a cluster of compressional events is identified on the northern side of the Enriquillo Lake (events 1, 3, 4, 5, 6 and 8; Fig. 5B), with a strike-slip component for event 6. Several studies have previously mapped an active thrust in this area (e.g., Pubellier et al., 2000), interpreted to be the active front of the Trans-Haitian fold and thrust belt. Our results confirm that this thrust is currently active and can produce M3.8 earthquakes or possibly larger.

Along the Septentrional-Oriente fault zone in the north, two thrust events are identified (events 23 and 7; Fig. 5A). Event 7 (4.5 km depth) is located along the on-land segment of the fault zone in Dominican Republic, which is transpressional (Calais et al., 1992b). The recent event of 7 October 2018 is similar to event 23 (Fig. 4): both are along the Septentrional-Oriente fault zone and thrust-fault related. The GEOSCOPE Observatory gives a magnitude of 5.9 and a depth of 28 km for the 7 October 2018 event, while we calculate a magnitude of 4.1 and a depth of 23 km for event 23. These depths of 28 and 23 km do not seem to correspond to crustal fault activity. Indeed, receiver functions studies made by González et al. (2012) and Corbeau et al. (2017) show that Moho is at ~20 km in the south of Cuba and 23 km in the north of Haiti. This activity under the Moho could be the effect of a slab edge push (van Benthem et al., 2014).








The P and T axes of the 26 focal mechanisms shown in the rose diagrams (Fig. 6) indicate that the principal compressional stress is trending N-S to NNE-SSW. This orientation is almost perpendicular to the trend of the strike-slip plate boundary in Haiti and is consistent with the results of Calais et al. (1992a) and Mejia and Pulliam (2018) for a large part of the plate boundary. This N-S compressional stress is interpreted to be the result of the collision between the Bahamas platform and Hispaniola. It differs from the generally ENE trend of relative motion in northern Hispaniola determined by GPS measurements

TABLE 2. FOCAL MECHANISMS CALCULATED IN THIS STUDY WITH THE TRANS-HAITI NETWORK DATASET

Event no.	Origin time yyymmdd hh:mm:ss.ss	Hypocenter			Centroid			Mlv	Mw	NP1			NP2			Mom Ten	DC%	VR%	NC	SNR	K°	CN
		Lat	Long	Depth	Lat	Long	Depth			Strike	Dip	Rake	Strike	Dip	Rake							
1	20130612 05:29:05.00	18.51	-71.55	3.0	18.56	-71.60	2.0	3.1	3.5	293	50	110	83	44	67		74.5	52	30	4	3.5	2.3
2	20130621 20:09:46.00	18.28	-71.63	2.1	18.26	-71.61	7.0	3.6	3.8	330	39	-82	140	52	-96		75.7	51	9	2	8	6.4
3	20130625 22:34:04.00	18.51	-71.53	2.9	18.50	-71.60	2.2	3	3.8	76	28	67	281	64	102		92.5	68	21	15	3.9	3.1
4	20130626 04:04:48.00	18.51	-71.54	2.5	18.54	-71.62	2.5	3.2	3.8	94	40	85	281	50	94		97.8	77	24	13	3	2.6
5	20130630 16:05:33.00	18.55	-71.60	-0.6	18.53	-71.57	2.0	3.1	3	99	10	79	290	80	92		83	36	9	6	6.4	4
6	20130712 10:22:04.00	18.51	-71.51	4.2	18.51	-71.51	3.0	3.3	3.4	69	64	149	174	63	30		38.7	35	12	7	6.9	3.7
7	20130718 01:54:39.00	19.74	-71.20	-1.8	19.69	-71.15	4.5	3.3	3.6	308	55	98	114	36	78		64.4	48	9	4	11.7	5.4
8	20130829 17:02:49.00	18.51	-71.58	-0.7	18.51	-71.58	2.5	2.7	3.1	138	32	137	266	69	66		86.3	45	9	16	6.5	1.6
9	20130922 02:25:25.00	18.47	-72.62	14.4	18.47	-72.62	13.0	2.7	3.1	153	87	170	243	80	3		63.4	51	15	2	16.3	9.2
10	20131012 17:59:15.00	18.48	-72.57	15.2	18.48	-72.55	10.7	2.8	3.5	76	50	-28	185	69	-137		94.7	42	15	5	5.6	3.1
11	20131221 23:07:20.00	18.14	-72.44	13.4	18.12	-72.47	26.8	2.8	4.4	64	70	132	175	46	29		35.6	82	12	32	5.3	4.2
12	20131222 04:48:49.00	18.13	-72.45	14.3	18.11	-72.46	26.6	2.7	3.6	190	57	36	78	61	141		60.3	45	12	3	4.6	4.5
13	20140123 03:16:16.00	18.34	-71.33	7.5	18.32	-71.27	12.5	3.2	3.6	296	19	-88	113	71	-91		66.7	39	12	3	3.7	3.3
14	20140201 11:29:26.00	18.21	-71.67	5.0	18.19	-71.75	9.5	3.3	3.5	105	70	95	271	20	76		81.2	37	9	5	7	4.7
15	20140212 23:20:55.0	18.53	-71.82	12.5	18.53	-71.82	18.0	3.8	3.7	25	62	-83	191	29	-102		98.2	43	12	12	5.3	3.5
16	20140313 20:34:53.00	18.68	-71.65	11.5	18.75	-71.73	3.5	2.9	2.9	24	22	-126	243	73	-77		90.7	53	9	2	4.4	2
17	20140322 01:11:40.32	18.52	-73.67	12.0	18.52	-73.63	7.0	3.9	4.2	285	53	96	95	38	82		74.3	49	27	2	3.6	3.8
18	20140510 18:27:22.00	18.38	-73.56	9.6	18.41	-73.53	17.6	3.3	3.9	334	63	-60	102	40	-135		47.7	60	12	3	12.5	5.7
19	20140526 09:18:11.00	18.42	-72.82	37.9	18.42	-72.86	18.0	2.5	3.9	226	27	-116	75	66	-78		36.9	62	12	8	5.5	3.9

Notes: DC%—double-couple percentage; VR%—variance reduction percentage; NC—number of components used; SNR—signal to noise ratio; K°—mean Kagan angle; CN—condition number; Mom Ten—Moment tensor.

TABLE 3. FOCAL MECHANISMS CALCULATED IN THIS STUDY WITH THE CUBAN NETWORK

Event no.	Origin time yyymmdd hh:mm:ss.ss	Hypocenter			Centroid			Mw	NP1			NP2			Mom Ten	DC%	VR%	NC	SNR	K°	CN
		Lat	Long	Depth	Lat	Long	Depth		Strike	Dip	Rake	Strike	Dip	Rake							
20	20150717 12:23:09.10	19.29	−73.69	33.0	19.21	−73.63	29.0	4.4	107	12	61	317	80	96		97.3	53	17	16	3.1	2.1
21	20151231 02:20:43.00	19.43	−73.63	10.0	19.40	−73.66	13.0	4.7	128	35	77	324	56	99		52.9	63	26	18	3.5	2.2
22	20160106 17:55:57.30	19.19	−73.08	23.0	19.19	−73.14	9.0	4.2	302	82	−86	93	9	−118		98.1	61	13	7	4.4	1.9
23	20160328 13:57:32.50	19.82	−73.86	10.0	19.96	−73.92	23.0	4.1	59	64	55	297	43	139		79.2	68	19	8	6.3	3.2
24	20161112 06:00:50.00	18.45	−74.24	31.0	18.47	−74.24	18.0	4	352	72	−161	256	72	−19		90	64	18	10	4.8	2.1
25	20170620 19:01:18.60	19.20	−74.18	5.0	19.20	−74.18	30.0	4.5	265	79	−85	60	12	−115		73.9	30	18	30	3.5	2.4
26	20170902 20:14:08.00	18.94	−72.05	15.7	18.83	−72.02	9.0	4.4	311	49	−45	74	58	−129		63.6	82	15	12	5.3	2.3

Notes: DC%—double-couple percentage; VR%—variance reduction percentage; NC—number of components used; SNR—signal to noise ratio; K°—mean Kagan angle; CN—condition number; Mom Ten—Moment tensor.

(e.g., Benford et al., 2012). Furthermore, the study of van Benthem et al. (2014) proposes that the slab edge push under Hispaniola was the dominant driver of the deformation since 30 Ma, in addition to collision with the Bahamas Platform. In their model, the western edge of the south-dipping Puerto Rico slab is moving sideways with the North American plate and produces westward deformation, dominating the collision-induced deformation. For the present, both slab edge push mechanism and Bahamas collision reproduce observations (van Benthem et al., 2014). Our results show that the present-day compression, trending N-S to NNE-SSW, more clearly reflects the collision with the Bahamas platform.

5.2 Seismicity and Crustal Structure

The year of seismicity recorded in this study is mostly located in the south of Haiti (Fig. 4). This can be explained by a higher rate of tectonic activity in the south of the island, with seismicity associated with the postseismic phase of the Mw 7.0 2010 earthquake (Possee et al., 2019).

Figure 7 shows several cross sections of the seismicity over the study area. The cross-section AA' represents the Gulf of Gonâve area, which is interpreted to be the offshore continuation of the onshore Trans-Haitian Belt, a well-known fold-and-thrust system on Hispaniola (Mann et al., 1995), where N120°E-trending, north-dipping active thrusts have been mapped by Pubelier et al. (2000). Corbeau et al. (2016) show with seismic-reflection profiles across the Gulf of Gonâve that there are active folding and thrusts in this area,

associated with thrust-fault ramps. The seismicity recorded offshore in the Gulf of Gonâve is distributed over the top 30 km of the crust and may correspond to the thrust-fault ramps inferred from the seismic-reflection profiles. Some intermediate-depth earthquakes are also recorded in this area and will be discussed below.

The transect CC' (Fig. 7) crosscuts the Cul-de-Sac Basin and the cluster of seismicity near Enriquillo Lake. The cross section shows that the seismicity is distributed between two thrusts facing each other, the northern side of the Southern Peninsula and the southern side of the Trans-Haitian belt. Between them there are few earthquakes and as shown by Symithe and Calais (2016), this diffuse seismicity does not confirm the presence of the Enriquillo-Plantain-Garden fault zone. Several intermediate-depth earthquakes are also recorded in this area and will be discussed in the following section.

The transect BB' (Fig. 7) crosscuts the whole of Haiti from the North Haitian fault in the north to the Southern Peninsula. We overlaid the crustal cross section of Corbeau et al. (2017) made from a receiver function study to indicate the transition between the crustal terranes (in blue, orange, and purple) and the mantle (in brown). The majority of the seismicity occurs in the crust, except several events in the southern part of the transect and intermediate-depth earthquakes under the entire cross section. A cluster of seismicity is present in the north, around the Septentrional-Oriente fault zone. On the enlargement (BB', Fig. 7) the transition between the Southern Peninsula and the Cul-de-Sac basin is marked by segments of the Enriquillo-Plantain-Garden fault zone. The seismicity is distributed at depth in the Southern Peninsula, while it is superficial and sparse in the Cul-de-Sac basin. A cluster of seismicity is identified

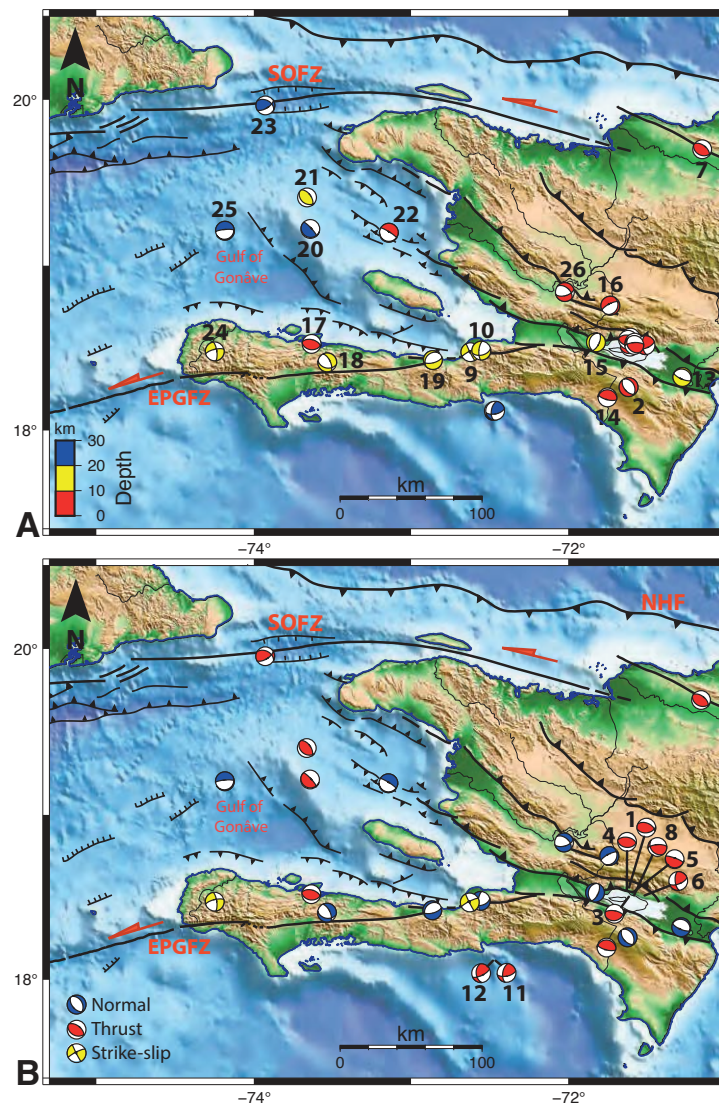


Figure 5. (A) Distribution of the focal mechanisms as a function of depth. (B) Distribution of the focal mechanisms as a function of slip type.

between the Enriquillo-Plantain-Garden segments and may be related to the activity following the 2010 earthquake. Moreover, a remarkable distribution of events just below the crust-mantle transition is identified (enlargement, BB'; Fig. 7) and seems to be a thrust ramp fault. Such a straight structure was previously proposed by Saint-Fleur et al. (2015).

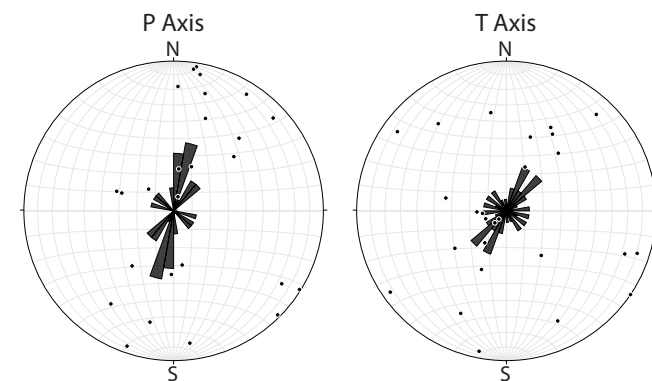


Figure 6. Rose diagrams for the P axis (left) and T axis (right) of the 26 focal mechanisms calculated in this study. The P and T axes indicate that the principal compressional stress is trending N-S to NNE-SSW.

5.3 Intermediate-Depth Earthquakes under Haiti

On the three cross sections shown in Figure 7, some intermediate-depth earthquakes are identified. These events have depths ranging from ~40 km to 260 km, and their depths increase southward. Such intermediate-depth seismicity can be related to the presence of a slab or a remnant slab under Haiti. Nevertheless, several authors have previously used the global seismicity and modeled the slab of the North American plate subduction and its edges and shown that its north-west edge is located in Dominican Republic (Calais et al., 1992a; van Benthem et al., 2013; Symithe et al., 2015; Harris et al., 2018). The deep seismicity reaching ~300 km under Puerto Rico and Dominican Republic is commonly interpreted as evidence for subducted North American lithosphere. For Calais et al. (1992a), the slab does not exist west of 70°30'W due to the lack of deep seismicity.

The new results from the Trans-Haiti network, even over a short time period, indicate that the previous interpretations of the western edge of the North American slab under Hispaniola should potentially be revised. The intermediate-depth earthquakes located in this study are most probably the result of a deep deformation caused by a slab or a remnant slab under Haiti. The lack of seismic stations and permanent network in this area likely made recording of such intermediate-depth seismicity difficult, thus influencing previous interpretations and modeling. A remnant slab is also expected to be less seismically active. According to Calais et al. (1992a), the slab is broken off west of Puerto Rico and is sinking into the mantle under Hispaniola. International Seismological Centre global catalogue and our results show that under Haiti, several intermediate-depth earthquakes are present (Fig. 8). Although we do not have enough events to form a clear Benioff zone on the cross section (DD', Fig. 8), these events are located at expected depths for a subducting slab or a remnant slab in this region (Symithe et al., 2015).

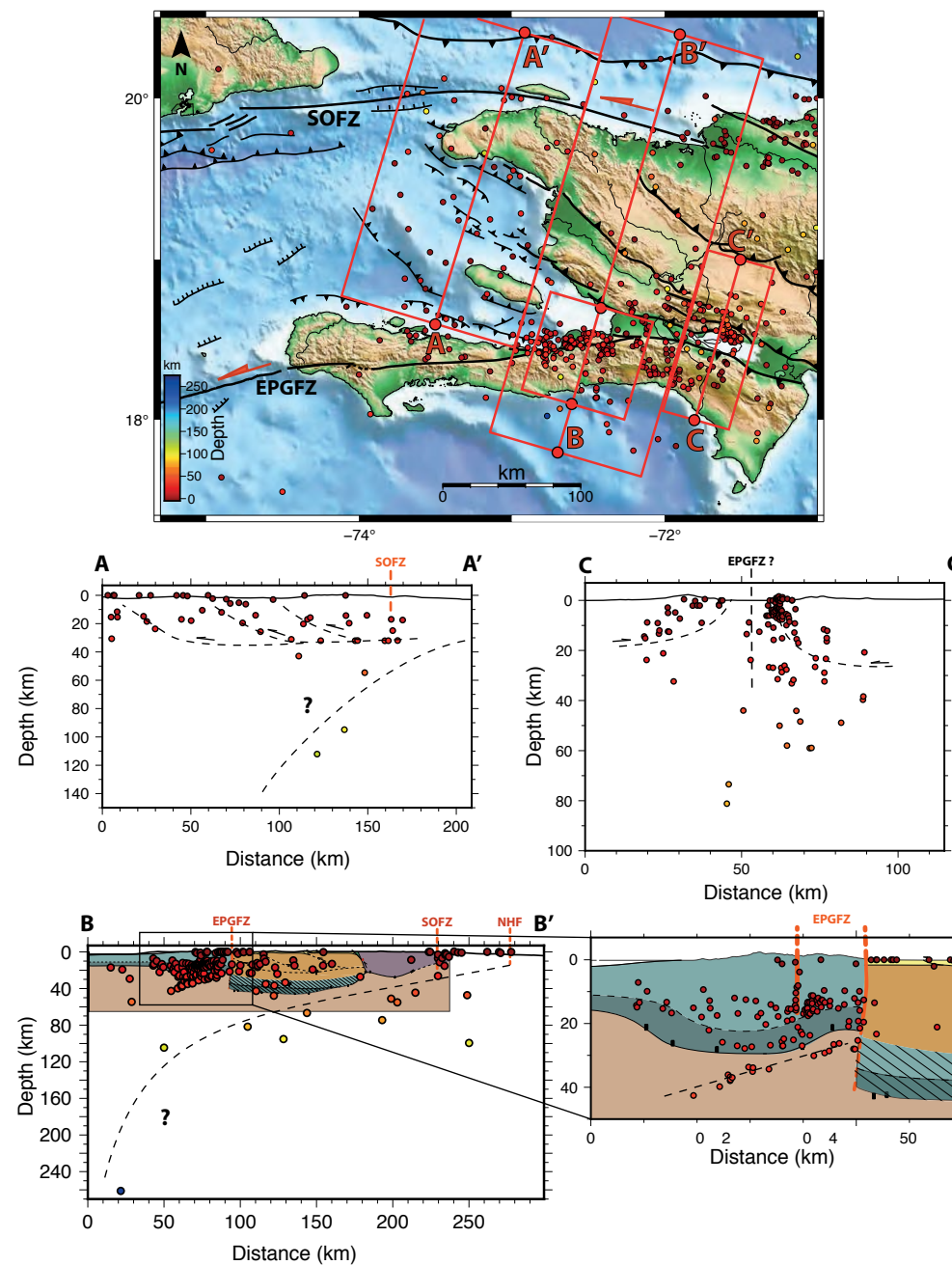


Figure 7. Cross sections of seismicity. NHF—North Haitian fault; SOFZ—Septentrional-Oriente fault zone; EPGFZ—Enriquillo-Plantain-Garden fault zone. On the CC' cross section and its enlargement, we overlaid the crustal cross section of Corbeau et al. (2017) made from a receiver function study. The crustal terranes are in blue, orange, and purple. The brown part represents the mantle.

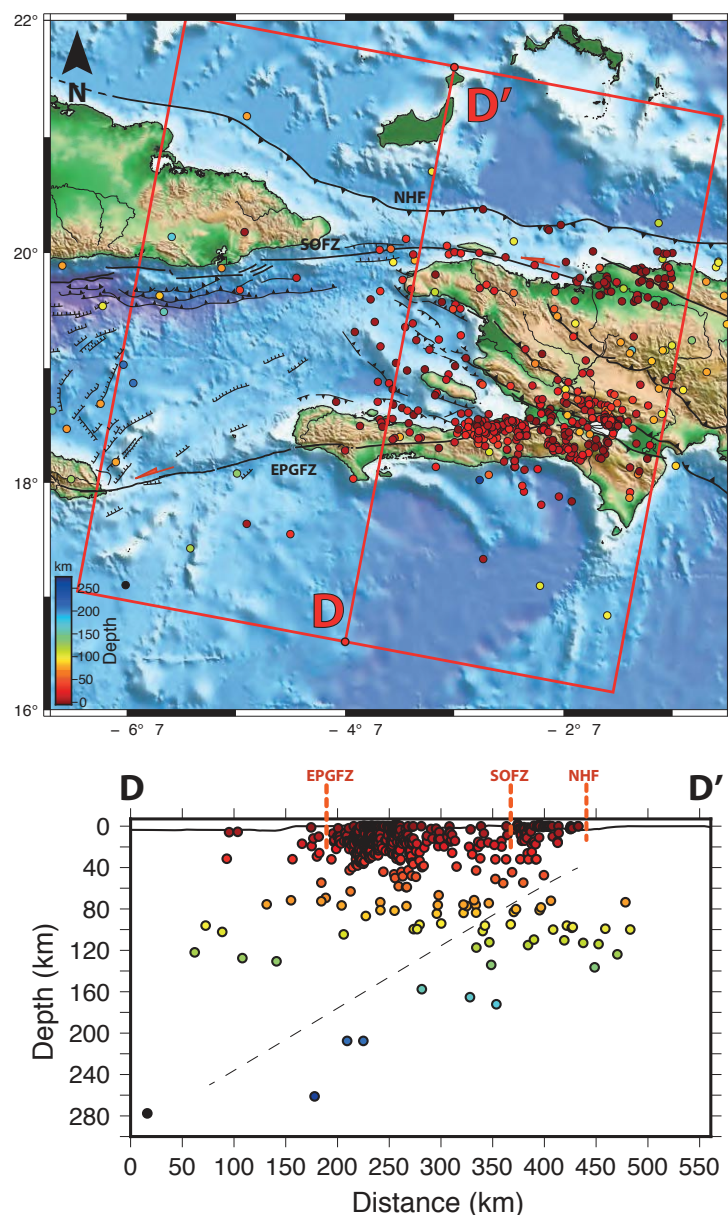


Figure 8. Local seismicity of this study superimposed on the International Seismological Center global reviewed catalog (seismicity from 1950 to 2005, hypocenters >70 km depth) and the associated cross section. NHF—North Haitian fault; SOFZ—Septentrional-Oriente fault zone; EPGFZ—Enriquillo-Plantain-Garden fault zone.

6. CONCLUSIONS

We analyze one year of local seismicity in Haiti from the Trans-Haiti temporary network. The new data set shows that the shallow seismicity is well correlated with known tectonic features. The most intense seismicity is located in the south of Haiti, near the 2010 earthquake epicenter and around the Cul-de-Sac basin, with a cluster of compressional earthquakes in the northern side of the Enriquillo Lake. Focal mechanisms are mainly compressional, and the mean compressional P axis is oriented N-S to NNE-SSW, suggesting that the current deformation is dominated by the collision between the Bahamas platform and Hispaniola. The presence of intermediate-depth earthquakes, ~40–260 km depth, below the Moho suggests the existence of a subducting slab (or possibly a remnant slab) inherited from the frontal subduction of the North American plate under Haiti.

ACKNOWLEDGMENTS

We thank Seismic Equipment Infra-Structure in the UK (SEIS-UK) for use of the instruments and their computing facilities. The facilities of SEIS-UK are supported by the Natural Environment Research Council (NERC) under agreement R8/H10/64. This research was partially supported by the European Interreg Caraïbe V program through the Plateforme Régionale de Surveillance Tellurique (or PREST) project. We are grateful to the team of the Observatoire Volcanologique et Sismologique de Martinique–Institut de Physique du Globe de Paris for the software provided for the data management. We thank the associate editor Laura Wallace and two anonymous reviewers for helpful comments that improved the manuscript.

REFERENCES CITED

- Benford, B., DeMets, C., and Calais, E., 2012, GPS estimates of microplate motions, northern Caribbean: Evidence for a Hispaniola microplate and implications for earthquake hazard: *Geophysical Journal International*, v. 191, no. 2, p. 481–490, <https://doi.org/10.1111/j.1365-246X.2012.05662.x>.
- Beyreuther, M., Barsch, R., Krischer, L., Megies, T., Behr, Y., and Wassermann, J., 2010, ObsPy: A Python Toolbox for Seismology: *Seismological Research Letters*, v. 81, no. 3, p. 530–533, <https://doi.org/10.1785/gssrl.81.3.530>.
- Bien-Aimé Momplaisir, R., 1986, Contribution à l'étude géologique de la partie orientale du Massif de la Hotte (Presqu'île du Sud d'Haïti): Synthèse structurale des marges de la presqu'île à partir de données sismiques [Ph.D. thesis]: Paris, Université Pierre et Marie Curie, 210 p.
- Boisson, D., 1987, Etude géologique du massif du nord d'Haïti (Hispaniola-grandes Antilles) [Ph.D. thesis]: Paris, Université Pierre et Marie Curie, 215 p.
- Bruña, J.G., Carbó-Gorostabel, A., Estrada, P.L., Muñoz-Martín, A., Ten Brink, U.S., Ballesteros, M.G., Druet, M., and Pazos, A., 2014, Morphostructure at the junction between the Beata ridge and the Greater Antilles island arc (offshore Hispaniola southern slope): *Tectonophysics*, v. 618, p. 138–163, <https://doi.org/10.1016/j.tecto.2014.02.001>.
- Burke, K., 1988, Tectonic evolution of the Caribbean: *Annual Review of Earth and Planetary Sciences*, v. 16, p. 201–230, <https://doi.org/10.1146/annurev.earth.16.050188.001221>.
- Calais, E., and Mercier de Lépinay, B., 1991, From transtension to transpression along the northern Caribbean plate boundary off Cuba: Implications for the recent motion of the Caribbean plate: *Tectonophysics*, v. 186, no. 3–4, p. 329–350, [https://doi.org/10.1016/0040-1951\(91\)90367-2](https://doi.org/10.1016/0040-1951(91)90367-2).
- Calais, E., Béthoux, N., and Mercier de Lépinay, B., 1992a, From transcurrent faulting to frontal subduction: A seismotectonic study of the northern Caribbean plate boundary from Cuba to Puerto Rico: *Tectonics*, v. 11, no. 1, p. 114–123, <https://doi.org/10.1029/91TC02364>.
- Calais, E., Mercier de Lépinay, B., Saint-Marc, P., Butterlin, J., and Schaaf, A., 1992b, La Limite de plaques décrochante nord caraïbe en Hispaniola; évolution paléogéographique et structurale cénozoïque: *Bulletin de la Société Géologique de France*, v. 163, no. 3, p. 309–324.
- Calais, E., Mazabraud, Y., Mercier de Lépinay, B., Mann, P., Mattioli, G., and Jansma, P., 2002, Strain partitioning and fault slip rates in the northeastern Caribbean from GPS measurements: *Geophysical Research Letters*, v. 29, no. 18, 1856, <https://doi.org/10.1029/2002GL015397>.

- Calais, E., Freed, A., Mattioli, G., Amelung, F., Jónsson, S., Jansma, P., Hong, S.-H., Dixon, T., Prépetit, C., and Momplaisir, R., 2010, Transpressional rupture of an unmapped fault during the 2010 Haiti earthquake: *Nature Geoscience*, v. 3, no. 11, p. 794–799, <https://doi.org/10.1038/ngeo992>.
- Corbeau, J., Rolandone, F., Leroy, S., Meyer, B., Mercier de Lépinay, B., Ellouz-Zimmermann, N., and Momplaisir, R., 2016, How transpressive is the Northern Caribbean plate boundary?: *Tectonics*, v. 35, no. 4, p. 1032–1046, <https://doi.org/10.1002/2015TC003996>.
- Corbeau, J., Rolandone, F., Leroy, S., Guerrier, K., Keir, D., Stuart, G., Clouard, V., Gallacher, R., Ulysse, S., and Boisson, D., Bien-aimé Momplaisir, R., Saint Preux, F., Prépetit, C., Saurel, J.-M., Mercier de Lépinay, B., and Meyer, B., 2017, Crustal structure of western Hispaniola (Haiti) from a teleseismic receiver function study: *Tectonophysics*, v. 709, p. 9–19, <https://doi.org/10.1016/j.tecto.2017.04.029>.
- Cruz-Orosa, I., Sàbat, F., Ramos, E., Rivero, L., and Vázquez-Taset, Y.M., 2012, Structural evolution of the La Trocha fault zone: Oblique collision and strike-slip basins in the Cuban orogen: *Tectonics*, v. 31, no. 5, <https://doi.org/10.1029/2011TC003045>.
- Dorel, J., 1978, Sismicité et structure de l'arc des Petites Antilles et du bassin Atlantique [Ph.D. thesis]: Paris, Université Pierre et Marie Curie, 326 p.
- Douilly, R., Haase, J.S., Ellsworth, W.L., Bouin, M.-P., Calais, E., Symithe, S.J., Armbruster, J.G., de Lépinay, B.M., Deschamps, A., Mildor, S.-L., Meremonte, M.E., and Hough, S.E., 2013, Crustal structure and fault geometry of the 2010 Haiti earthquake from temporary seismometer deployments: *Bulletin of the Seismological Society of America*, v. 103, no. 4, p. 2305–2325, <https://doi.org/10.1785/0120120303>.
- Escuder Viruete, J., Contreras, F., Stein, G., Urien, P., Joubert, M., Ullrich, T.D., Mortensen, J., and Perez Estaun, A., 2006, Transpression and strike-slip partitioning in the Caribbean island arc: Fabric development, kinematics and Ar-Ar ages of syntectonic emplacement of the Loma de Cabrera batholith, Dominican Republic: *Journal of Structural Geology*, v. 28, p. 1496–1519, <https://doi.org/10.1016/j.jsg.2006.04.003>.
- González, O.L., Moreno, B., Romanelli, F., and Panza, G.F., 2012, Lithospheric structure below seismic stations in Cuba from the joint inversion of Rayleigh surface waves dispersion and receiver functions: *Geophysical Journal International*, v. 189, no. 2, p. 1047–1059, <https://doi.org/10.1111/j.1365-246X.2012.05410.x>.
- Graves, R.W., and Pitarka, A., 2010, Broadband ground-motion simulation using a hybrid approach: *Bulletin of the Seismological Society of America*, v. 100, no. 5A, p. 2095–2123, <https://doi.org/10.1785/0120100057>.
- Hanka, W., Saul, J., Weber, B., Becker, J., Harjadi, P., Fauzi, and GITEWS Seismology Group, 2010, Real-time earthquake monitoring for tsunami warning in the Indian Ocean and beyond: *Natural Hazards and Earth System Sciences*, v. 10, p. 2611–2622, <https://doi.org/10.5194/nhess-10-2611-2010>.
- Harris, C.W., Miller, M.S., and Porritt, R.W., 2018, Tomographic Imaging of Slab Segmentation and Deformation in the Greater Antilles: *Geochemistry, Geophysics, Geosystems*, v. 19, no. 8, p. 2292–2307, <https://doi.org/10.1029/2018GC007603>.
- International Seismological Centre, 2016, On-line Bulletin, <http://www.isc.ac.uk>, <https://doi.org/10.31905/D808B830>.
- Iturralde-Vinent, M.A., 2006, Meso-Cenozoic Caribbean paleogeography: Implications for the historical biogeography of the region: *International Geology Review*, v. 48, no. 9, p. 791–827, <https://doi.org/10.2747/0020-6814.48.9.791>.
- Křížová, D., Zahradník, J., and Kiratzi, A., 2013, Resolvability of isotropic component in regional seismic moment tensor inversion: *Bulletin of the Seismological Society of America*, v. 103, no. 4, p. 2460–2473, <https://doi.org/10.1785/0120120097>.
- Lee, W.H.K., and Lahr, J.C., 1972, HYPO71: A computer program for determining hypocenter, magnitude, and first motion pattern of local earthquakes: U.S. Geological Survey Open-File Report 72-224, 100 p., <https://doi.org/10.3133/ofr72224>.
- Leroy, S., Mercier de Lépinay, B., Mauffret, A., and Pubellier, M., 1996, Structural and tectonic evolution of the eastern Cayman Trough (Caribbean Sea) from seismic reflection data: *American Association of Petroleum Geologists Bulletin*, v. 80, no. 2, p. 222–247.
- Leroy, S., Mauffret, A., Patriat, P., and Mercier de Lépinay, B., 2000, An alternative interpretation of the Cayman trough evolution from a reidentification of magnetic anomalies: *Geophysical Journal International*, v. 141, no. 3, p. 539–557, <https://doi.org/10.1046/j.1365-246x.2000.00059.x>.
- Leroy, S., Ellouz-Zimmermann, N., Corbeau, J., Rolandone, F., Mercier de Lépinay, B., Meyer, B., Momplaisir, R., Granja Bruña, J.-L., Battani, A., Baurion, C., Burrov, E., Clouard, V., Deschamps, R., Gorini, C., Hamon, Y., Lafosse, M., Leonel, J., Le Pourhiet, L., Llanes Estrada, P., Loget, N., Lucazeau, F., Pillot, D., Poort, J., Tankoo, K.R., Cuevas, J.-L., Alcaide, J.-F., Poix, C.J., Muñoz-Martin, A., Mitton, S., Rodriguez, Y., Schmitz, J., Seeber, L., Carbo-Gorosabel, A., and Muñoz, S., 2015, Segmentation and kinematics of the North America–Caribbean plate boundary offshore Hispaniola: *Terra Nova*, v. 27, no. 6, p. 467–478, <https://doi.org/10.1111/ter.12181>.
- Lomax, A., Virieux, J., Volant, P., and Berge, C., 2000, Probabilistic earthquake location in 3D and layered models: Introduction of a Metropolis-Gibbs method and comparison with linear locations, in Thurber, C.H., and Rabinowitz, N., eds., *Advances in Seismic Event Location, Modern Approaches in Geophysics*: Dordrecht, Springer, v. 18, p. 101–134, https://doi.org/10.1007/978-94-015-9536-0_5.
- Mann, P., Taylor, F., Edwards, R.L., and Ku, T.-L., 1995, Actively evolving microplate formation by oblique collision and sideways motion along strike-slip faults: An example from the north-eastern Caribbean plate margin: *Tectonophysics*, v. 246, no. 1, p. 1–69, [https://doi.org/10.1016/0040-1951\(94\)00268-E](https://doi.org/10.1016/0040-1951(94)00268-E).
- Mauffret, A., and Leroy, S., 1999, Neogene Intraplate Deformation of the Caribbean Plate at the Beata Ridge, in Mann, P., ed., *Caribbean Basins: Sedimentary Basins of the World*: Elsevier, v. 4, p. 627–669, [https://doi.org/10.1016/S1874-5997\(99\)80055-0](https://doi.org/10.1016/S1874-5997(99)80055-0).
- McCann, W.R., and Sykes, L.R., 1984, Subduction of aseismic ridges beneath the Caribbean plate: Implications for the tectonics and seismic potential of the northeastern Caribbean: *Journal of Geophysical Research. Solid Earth*, v. 89, no. B6, p. 4493–4519, <https://doi.org/10.1029/JB089iB06p04493>.
- Mejia, H., and Pulliam, J., 2018, P-and T-Axis Probabilities (PaTaPs): Characterizing Regional Stress Patterns with Probability Density Functions of Fault-Plane Uncertainties: *Seismological Research Letters*, v. 89, no. 6, p. 2354–2361, <https://doi.org/10.1785/0220180112>.
- Mercier de Lépinay, B., Deschamps, A., Klingelhoefer, F., Mazabraud, Y., Delouis, B., Clouard, V., Hello, Y., Crozon, J., Marcaillou, B., Graindorge, D., Vallée, M., Perrot, J., Bouin, M.-P., Saurel, J.-M., Charvis, P., and St-Louis, M., 2011, The 2010 Haiti earthquake: A complex fault pattern constrained by seismologic and tectonic observations: *Geophysical Research Letters*, v. 38, L22305, <https://doi.org/10.1029/2011GL049799>.
- Nafe, J.E., and Drake, C.L., 1960, Physical properties of marine sediments, in Hill, M.N., ed., *The Sea*: New York, Wiley-Interscience, v. 3, p. 794–815.
- Pindell, J., Kennan, L., Stanek, K.P., Maresch, W.V., and Draper, G., 2006, Foundations of Gulf of Mexico and Caribbean evolution: Eight controversies resolved: *Geologica Acta*, v. 4, no. 1, p. 303–341.
- Possee, D., Keir, D., Harmon, N., Rychert, C., Rolandone, F., Leroy, S., Corbeau, J., Stuart, G., Calais, E., Illsley-Kemp, F., Boisson, D., Momplaisir, R., and Prépetit, C., 2019, The tectonics and active faulting of Haiti from seismicity and tomography: *Tectonics*, <https://doi.org/10.1029/2018TC005364>.
- Pubellier, M., Mauffret, A., Leroy, S., Vila, J.M., and Amicar, H., 2000, Plate boundary readjustment in oblique convergence: Example of the Neogene of Hispaniola, Greater Antilles: *Tectonics*, v. 19, no. 4, p. 630–648, <https://doi.org/10.1029/2000TC900007>.
- Saint Fleur, N., Feuillet, N., Grandin, R., Jacques, E., Weil-Accardo, J., and Klinger, Y., 2015, Seismotectonics of southern Haiti: A new faulting model for the 12 January 2010 M7 earthquake: *Geophysical Research Letters*, v. 42, no. 23, p. 10,273–10,281, <https://doi.org/10.1002/2015GL065505>.
- Sokos, E.N., and Zahradník, J., 2008, ISOLA a Fortran code and a Matlab GUI to perform multiple-point source inversion of seismic data: *Computers & Geosciences*, v. 34, no. 8, p. 967–977, <https://doi.org/10.1016/j.cageo.2007.07.005>.
- Sokos, E.N., and Zahradník, J., 2013, Evaluating centroid-moment-tensor uncertainty in the new version of ISOLA software: *Seismological Research Letters*, v. 84, no. 4, p. 656–665, <https://doi.org/10.1785/0220130002>.
- Symithe, S., and Calais, E., 2016, Present-day shortening in Southern Haiti from GPS measurements and implications for seismic hazard: *Tectonophysics*, v. 679, p. 117–124, <https://doi.org/10.1016/j.tecto.2016.04.034>.
- Symithe, S., Calais, E., Chabaliere, J.B., Robertson, R., and Higgins, M., 2015, Current block motions and strain accumulation on active faults in the Caribbean: *Journal of Geophysical Research. Solid Earth*, v. 120, p. 3748–3774, <https://doi.org/10.1002/2014JB011779>.
- van Benthem, S., Govers, R., Spakman, W., and Wortel, R., 2013, Tectonic evolution and mantle structure of the Caribbean: *Journal of Geophysical Research. Solid Earth*, v. 118, no. 6, p. 3019–3036, <https://doi.org/10.1002/jgrb.50235>.
- van Benthem, S., Govers, R., and Wortel, R., 2014, What drives microplate motion and deformation in the northeastern Caribbean plate boundary region?: *Tectonics*, v. 33, no. 5, p. 850–873, <https://doi.org/10.1002/2013TC003402>.
- Wang, J., Mann, P., and Stewart, R.R., 2018, Late Holocene structural style and seismicity of highly transpressional faults in southern Haiti: *Tectonics*, <https://doi.org/10.1029/2017TC004920>.
- Zahradník, J., and Custódio, S., 2012, Moment tensor resolvability: Application to southwest Iberia: *Bulletin of the Seismological Society of America*, v. 102, no. 3, p. 1235–1254, <https://doi.org/10.1785/0120110216>.